

ACTIVE CONTOURS WITH OPTICAL FLOW AND PRIMITIVE SHAPE PRIORS FOR ECHOCARDIOGRAPHIC IMAGERY

Ali K. Hamou and Mahmoud R. El-Sakka

Department of Computer Science, University of Western Ontario, London, Ontario, N6A 5B7, Canada

Keywords: Active contours, Deformable models, Snakes, Gradient vector flow, Shape priors, Optical flow, Echocardiography.

Abstract: Accurate delineation of object borders is highly desirable in echocardiography. Among other model-based techniques, active contours (or snakes) provide a unique and powerful approach to image analysis. In this work, we propose the use of a new external energy for a GVF snake, consisting of the optical flow data of moving heart structures (i.e. the perceived movement). This new external energy provides more information to the active contour model to combat noise in moving sequences. An automated primitive shape prior mechanism is also introduced, which further improves the results when dealing with especially noisy echocardiographic image cines. Results were compared with that of expert manual segmentations yielding promising sensitivities and system accuracies.

1 INTRODUCTION

Echocardiography, imaging the heart using ultrasound waves, has become the most widely used modality to observe heart motion and deformation over other modalities (e.g. Positron Emission computed Tomography, Cardiac Magnetic Resonance, Computer Tomography). This is due to the relatively inexpensive cost of the technology along with its non-invasive nature, yielding no known side-effects. Sophisticated enhancements to the acquisition devices over the years have yielded real-time dynamic observation of heart function.

Unfortunately, US data still suffers from speckle noise. It may also exhibit occluded borders due to the erratic scattering of its impinging waves (once it encounters various tissue densities). Efforts have been made to compensate for these shortcomings, including filtering (Mazumdar, 2006) and incorporating the speckle noise effect directly into the algorithm (Tauber et al., 2008). Regardless, boundary detection techniques need to be employed in order to segment a region of interest (ROI). Analysis of these segmented regions has led to various works on endocardial borders (Choy and Jin, 1996), stress and strain of the septum (Montagnat and Delingette, 2000), and wall motility (Amini et al., 1998), which all help to accurately diagnose cardiomyopathies.

Many computer vision techniques have been introduced in order to accomplish boundary detection. One such example is the active contour model, also commonly known as snakes (Kass et al., 1988).

Active contours treat the surface of an object as an elastic sheet that stretches and deforms when external and internal forces are applied to it. These models are physically-based, since their behavior is designed to mimic the physical laws that govern real-world objects, (Cohen, 1991). Since this approach relied on variational calculus to find a solution, time complexity was a major drawback. Amini et al. (1990) and Williams and Shah (1992) proposed algorithms that reduced time complexity making the active contour model feasible for segmentation systems.

Issues with large capture ranges (the failure of curve migration when initialized distant from the ROI to segment) and concavities (high internal energies may inhibit the capture of smaller features) are solved by other advances, which include inflation forces (Cohen and Cohen, 1993), probabilistic models (Mallouche et al., 1995), oriented particles (Szeliski and Tonnesen, 1992), and gradient vector flows (GVF) (Xu and Prince, 2000). For the purposes of this study, focus will be placed on those advances best suited for echocardiographic images.

Since the left ventricle represents one of the most important heart functions, many semi-automatic techniques have attempted to segment this region from its surrounding tissue.

Papademetris et al. (1999) proposed to measure the stress and strain of cardiac regional deformation of the left ventricle in ultrasound images by using a Markov random field (Kindermann and Snell, 1980). Texture data was incorporated into their model for use with a tracking algorithm. However, assumptions of uncorrelated data within their model are made (which may lead to a misclassification of structures due to noise) and complex calculations result in long computation times.

Eusemann el al. (2002) proposed the use of a modality independent quantitative visualization of the peak velocities. Though set manually, the technique utilizes a set of polygon meshes to deform by means of the anatomical centerline of the left ventricle.

Jolly (2003) proposed a semi-automatic segmentation algorithm with the use of three manually placed landmarks in order to estimate the location of various shape models. However, this system was designed for use on the end-systole and end-diastole images only, rather than the entire cardiac cycle.

Felix-Gonzalez and Valdes-Cristerna (2006) proposed a technique using a series of standard algorithms (e.g. mean shift filtering, edge mapping, entropy extraction and confidence mapping) along with an active surface model in order to deal with the speckle. This model is made up of cubic splines and is based on gradient descent, however no explanation is given on parameterization and how the empirical data was set.

Zhou el al. (2004) proposed the segmentation of MRI cardiac sequences using a generalized fuzzy GVF map along with a relative optical flow field. Optical flow measurements are computed on the cardiac sequence and a maximum a posteriori probability (MAP) is used as a window for the movement of the curve. The use of optical flow with GVF provides promising results, however since this technique is used exclusively on MRI data, there is no guarantee that it would work with US data given the presence of speckle noise.

In practice, many of the stated segmentation algorithms can be used on normal echocardiographic data. This is true given an adequate amount of user intervention and when such data exhibits low levels of speckle noise (i.e. from newer machines generally found in a research environment under ideal conditions with healthy volunteers). However in a

clinical setting, the objective is to be able to accurately identify myocardial borders on problematic echocardiograms with minimal time.

In this paper, we will present an external energy for GVF snakes that takes advantage of the motion data within echocardiographic image cines. Furthermore, we incorporate the use of primitive shape priors such that the contour placement will improve, especially when dealing with noisy regions and improper initialization.

The rest of the paper is organized as follows. Background information on relevant models will be briefly described in Section 2. The proposed scheme will be outlined in Section 3. Section 4 and Section 5 will contain the experimental results and conclusions, respectively.

2 BACKGROUND

2.1 Active Contours

A snake is an energy minimization problem. Its energy is represented by two forces (internal energy, E_{in} , and external energy, E_{ex}) which work against (or independent of) each other. The total energy should converge to a local minimum; ideally at the desired boundary. A snake can be parametrically defined as $v(s) = [x(s), y(s)]^T$, where s belongs to the interval $[0,1]$. Hence, the total energy to be minimized, E_{AC} , to give the best fit between a snake and a desired object shape is:

$$E_{AC} = \int_0^1 E_{in}(v(s)) + E_{ex}(v(s)) ds \quad (1)$$

where E_{in} decreases as the curve becomes smooth and E_{ex} decreases as it approaches the ROI, such as image structures or edges (i.e. areas of high gradient information).

As in Kass et al. (1988) the internal energy of the active contour formulation is further defined as:

$$E_{in}(v(s)) = \alpha(s) \times \left| \frac{dv}{ds} \right|^2 + \beta(s) \times \left| \frac{d^2v}{ds^2} \right|^2 \quad (2)$$

where $\alpha(s)$ and $\beta(s)$ are weighting factors of elasticity and stiffness, respectively. The first order term encourages the snake's surface to act like a membrane, whereas the second order term encourages the snake to act like a thin plate. $\alpha(s)$ controls the tension along the spine (stretching a balloon or elastic band) whereas $\beta(s)$ controls the rigidity of the spine (bending a thin plate or wire).

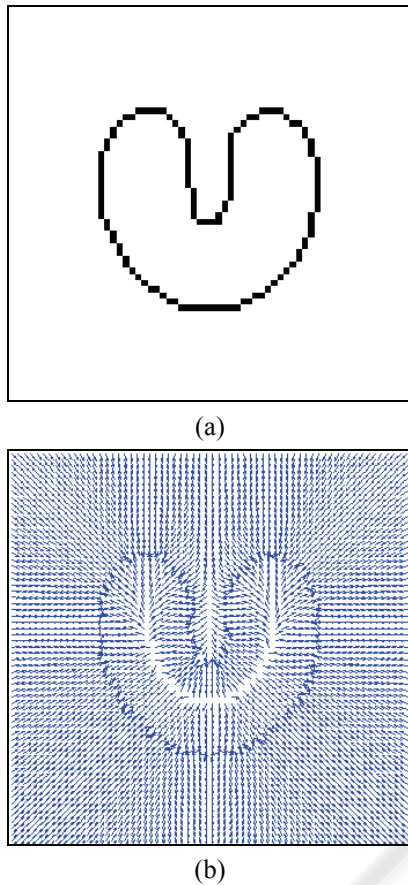


Figure 1: An example of the virtual electric field; (a) standard U-Image; (b) virtual electric field of image shown in (a).

A typical external energy formulation for a given image, $I(x,y)$, to identify edges is:

$$E_{ex}(x,y) = -|\nabla I(x,y)|^2 \quad (3)$$

where ∇ denotes the gradient operator. In the case of a noisier image the edges are further smoothed:

$$E_{ex}(x,y) = -|\nabla[G_\sigma(x,y)*I(x,y)]|^2 \quad (4)$$

where $G_\sigma(x,y)$ is a two-dimensional Gaussian function with standard deviation σ , and $*$ denotes a convolution operator. σ must be large enough to compensate for the image noise that would interfere with the active contour's capture range (the contour may get trapped by the noisy areas of the image).

The standard snake algorithm suffers from poor range due to initialization and the inability to capture concavities. Xu and Prince (2000) largely solved this problem by the advent of the GVF snake, which provides a field for guiding the contour to regions of high gradient. The GVF field is used as an external

energy and is characterized by the vector field $z(x,y)=[u(x,y),v(x,y)]$ that minimizes the energy functional:

$$\begin{aligned} E_{GVF} = & \iint \mu \times (|\nabla u|^2 + |\nabla v|^2) dx dy \\ & + \iint |\nabla f|^2 \times |z - \nabla f|^2 dx dy \end{aligned} \quad (5)$$

where $f = -E_{ex}$ is an edge map derived from the image and μ is the degree of smoothness of the field. Figure 1 shows an example of a GVF field on a standard U-Image.

2.2 Optical Flow

Optical flow approximates the apparent motion of an object over a series of images (or time). The relationship between the optical flow in the image plane and the velocities of objects in the three dimensional world is not necessarily obvious (Barron et al., 1994). For the sake of convenience, most optical flow techniques consider a particularly simple world where the apparent velocity of brightness patterns can be directly identified with the movement of surfaces in the scene. This implies that objects maintaining structure but changing intensity would break this assumption.

Consider an image intensity, $I(x,y,t)$ at time t . Time, in this instance, implies that next frame in an image cine. Assuming that at a small distance away, and some time later the given intensity is:

$$\begin{aligned} I(x+\Delta x, y+\Delta y, t+\Delta t) = & I(x, y, t) \\ & + \frac{\partial I}{\partial x} \Delta x + \frac{\partial I}{\partial y} \Delta y + \frac{\partial I}{\partial t} \Delta t + \text{higher order terms} \end{aligned} \quad (6)$$

Given that the object started at position (x,y) at time t , and that it moved by a small distance of $(\Delta x, \Delta y)$ over a period of Δt , the following assumption can be made:

$$I(x+\Delta x, y+\Delta y, t+\Delta t) = I(x, y, t) \quad (7)$$

The assumption in (7) would only be true if the intensity of our object is the same at both time t and $t + \Delta t$. Furthermore, if our Δx , Δy and Δt are very small, our higher order terms would vanish:

$$\frac{\partial I}{\partial x} \Delta x + \frac{\partial I}{\partial y} \Delta y + \frac{\partial I}{\partial t} \Delta t = 0 \quad (8)$$

Hence dividing (8) by Δt will yield:

$$-\frac{\partial I}{\partial t} = \frac{\partial I}{\partial x} \frac{\Delta x}{\Delta t} + \frac{\partial I}{\partial y} \frac{\Delta y}{\Delta t} \quad (9)$$

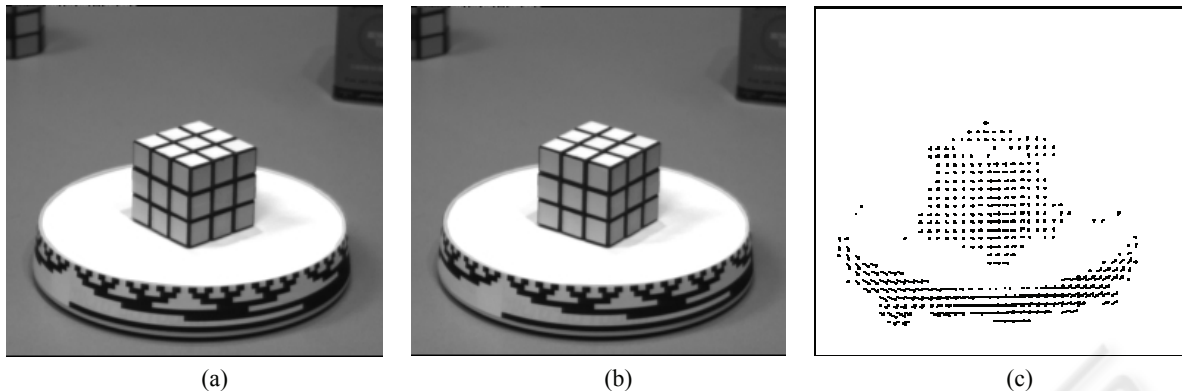


Figure 2: An example of an optical flow field on a Rubik's cube rotated image; (a) Rubik's cube at time t ; (b) Rubik's cube at time $t+\Delta t$; (c) optical flow.

$$-I_t = \frac{\partial I}{\partial x}u + \frac{\partial I}{\partial y}v, \quad (10)$$

where $u = \frac{\Delta x}{\Delta t}$ and $v = \frac{\Delta y}{\Delta t}$.

The equation in (10) is known as the optical flow constraint equation, where I_t at a particular pixel location, (x,y) , is how fast its intensity is changing with respect to time, u and v are the spatial rates of change for any given pixel (i.e. how fast an intensity is moving across an image). However, effectively estimating the component of the flow (along with intensity values) cannot directly be solved in this form since it will yield one equation per pixel for every two unknowns, u and v . In order to do so, additional constraints must be applied to this equation.

Horn and Schunck (1981) introduced a method for solving this problem using partial derivatives. A global regularization constraint is used which assumes that images consist of objects undergoing rigid motion, and so over relatively large areas the optical flow will be smooth. Figure 2 depicts a visual representation of the optical flow of a simple Rubik's cube. Note that the grayscale image has few shadows. This helps to maintain consistency in the luminance of each pixel which in turn yields accurate results.

3 DESCRIPTION OF PROPOSED MODEL

The use of the GVF snake directly on echocardiograms will not provide an adequate solution due to the complication of noise and other valves that exist within the heart cavity. Hence our scheme will make use of a GVF snake with optical

flow measurements. These measurements will be included in E_{GVF} .

By considering each image cine within an echocardiographic video loop, the Horn-Schunck technique is applied in order to detect the motion between various heart structures. These optical flow measurements will further filter noise from the cines since speckle tends to be stable throughout an image. As such, noise will be assigned smaller magnitudes of movement over surrounding structures and hence will be eliminated.

The magnitude of these optical flow estimates are then median filtered and the canny edge map (Canny, 1986) is extracted in order to generate the GVF field for the snake's external energy.

Since the generation of the GVF field is computationally prohibitive using real world data, the external energy is generated using a *virtual electric field* (VEF) of the preprocessed edge map (Park and Chung, 2002). The VEF is defined by considering each edge as a point charge within an electric field. This can be accomplished by convolving the edge map with the following two masks:

$$g_x(x, y) = \frac{-x}{4\pi\varepsilon \times (x^2 + y^2)^{3/2}} \quad (11)$$

$$g_y(x, y) = \frac{-y}{4\pi\varepsilon \times (x^2 + y^2)^{3/2}} \quad (12)$$

where ε is sufficiently small. Given a sufficient mask size, the resulting field yields a vector flow identical to the GVF field defined in (5), without the high computational cost. For instance, the vector field shown in Figure 1 was generated with (11) and (12) with a mask size of 32.

Since many of the anatomical structures (such as the left ventricle of the heart) are known shapes and

sizes, prior knowledge information can be directly used to increase the performance of a segmentation algorithm.

Priors based on shape statistical models require modifications to the standard active contour model. An iterative solution can be directly incorporated into any optimization model by using the proposed framework first outlined by Hamou et al. (2007).

Since it is desirable to incorporate shape priors into the model without directly involving the user, automated shape detection takes place on the set of discrete snake points, $v(s)$. This is achieved by replacing E_{ex} of our active contour with a least squares fit polynomial (specifically a third order hyperbola) of the current $v(s)$ points. This allows the fitting of a primitive shape (or a series of primitives as needed for the left ventricle) to the curve set $v(s)$. This will help compensate for the noise that inhibits the snake from migrating past a certain point. The user is able to increase or decrease the effect of the prior knowledge to the snake's convergence cycle.

Depending on the feature of interest to be segmented, different primitive priors can be used in order to improve the robustness of the technique. The priors are not limited to hyperbolas; rather a range of shapes can be selected by the user in order to best fit their feature of interest. This is useful in the medical arena where a specialist has a clear understanding of the underlying structure being detected, such as a liver, an artery, or a heart. A desired primitive shape can be selected before curve evolution takes place.

Figure 3 portrays the means of generating a primitive prior for the left ventricle of the 4 chamber view US heart image. The left ventricle points were split into an upper region and a lower region representing two separate shape fitting equations. This can be tuned to give the best prior by selecting the separation line of the regions with the least amount of distance between the fitted hyperbolas and snake curve. Further advantages are that the prior knowledge is not built on a set of training samples that are expert delineated; rather they are generated from the current active contour control points. Figure 4 shows the results of the prior generation scheme on a echocardiogram.

Once the prior is constructed, a VEF is generated of the prior and a single optimization iteration of the snake is executed before returning to the original optimization cycle. This is referred to as an *omega* iteration. This interruption to the snake optimization

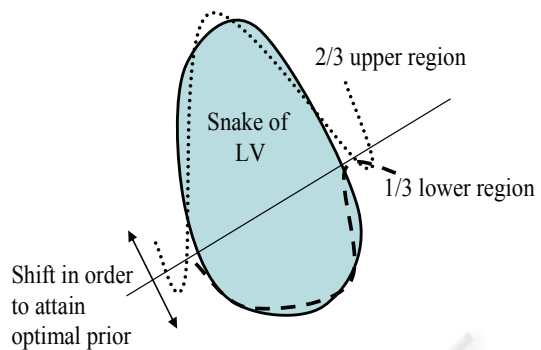


Figure 3: Generation of primitive priors on active contour points.

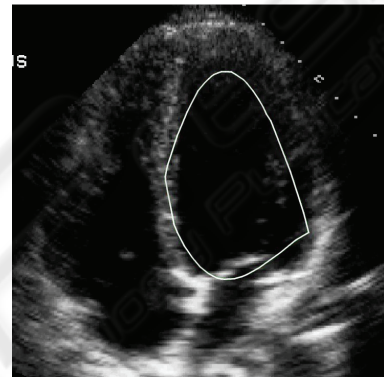


Figure 4: An example of a primitive prior formulation on the left ventricle.

cycle is repeated throughout the snake's evolution, until it achieves equilibrium. A flow chart of the proposed scheme is shown in Figure 5.

4 EXPERIMENTAL RESULTS

For this study, a series of B-mode echocardiogram cross sectional videos of the heart have been used to investigate the proposed snake algorithm. These videos were acquired using a SONOS 5500 by Philips Medical System. The transducer frequency was set at 2.5 Mhz in order to insure adequate penetration of tissue, while maintaining image quality with the existing speckle noise. Longitudinal views of the heart, which visualize the left ventricle, were acquired in order to verify the prior knowledge algorithm using more than one primitive shape.

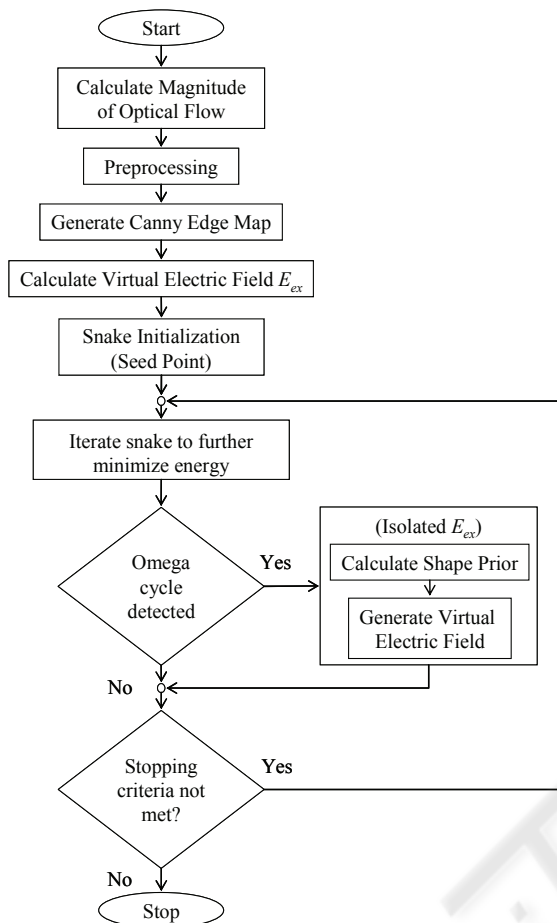
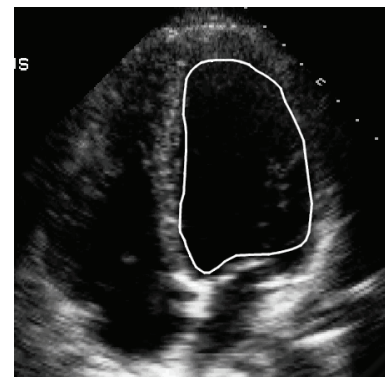


Figure 5: Flow Chart of Proposed Algorithm.

The videos were parsed into image cines and each frame was considered with its direct neighbouring frame. Optical flow calculations for the edge map were completed using the Horn-Schunck technique with a regularization constraint of 0.05 in order to compensate for the general speckle throughout the US images. Mask size for VEF generation was set to 64 and was normalized for active contour use. The initial contour placement was set to a circle of radius 30, which was placed by the user within the left ventricle of the heart.

Snake parameters, α and β , were set to 4 and 0, respectively. α was set to 4 in order to add a substantial amount of weight to the internal energy. β was set to 0 since the second order differential does not influence the snake enough to warrant the added time complexity. Priors (*omega* iteration) were invoked every five iterations of the snake minimization.

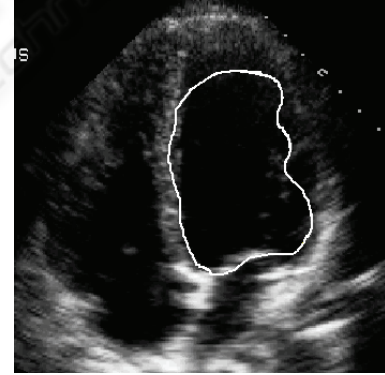
Figure 6(a) shows an expert manual segmentation of the left ventricle of the heart. Figure 6(b) shows the final contour using the traditional



(a)



(b)



(c)

Figure 6: Segmenting the left ventricle of the heart; (a) Expert manual segmentation (b) standard GVF segmentation (c) GVF-optical flow segmentation with priors.

GVF snake. Figure 6(c) shows the final contour using the optical flow GVF snake with primitive priors. Expert examination of the results reveals that the shape priors improve regularity by allowing the snake to overcome noise, artifacts. This allows for proper delineation of the left ventricular endocardial lining. The optical flow measurements provide the necessary structural information used in the external

energy of the snake.

Experiments were run on a complete cardiac cycle with various external energies. The first consisting purely of the optical flow measurements, the second on a combined energy of image gradient vectors and optical flow data.

Overall, accuracy of the proposed system was measured by comparing the 87 indexed images to the expert manual segmentations by a clinician. These measurements include both type I and type II errors as defined by Neyman and Pearson (1928). Since the images were mainly small segmented foregrounds against vast backgrounds, the system would best be measured by means of its sensitivity and system accuracy.

Sensitivity is the number of true positives divided by the number of true positives plus false negatives. System accuracy is the number of true positives and true negatives divided by the total number of pixels in the image. In other words, it classifies how accurate the results of the test are versus the total image.

The sensitivity of the system, given a 95% confidence interval, yields 0.568-0.610 when using the optical flow exclusively. However this yield increased to 0.722-0.759 when combined with a image gradient vectors. Whereas, system accuracy, given the same confidence interval, yields 0.940-0.946 for the optical flow energy and 0.954-0.958 for the combined energy, respectively.

Figure 7 shows the sensitivity of the system using various energies. Figure 8 shows the system accuracy of the system. We notice that there is a slight improvement when segmenting using both the optical flow and the image gradient over the optical flow exclusively. This illustrates that the optical flow measurements contributes enough information to the snake in order to segment out the left ventricle.

5 CONCLUSIONS

In this paper, we have shown that the use of optical flow calculations can be used as an external energy within the GVF active contour framework. By exclusively using the optical flow calculations, we have shown that it is possible that an active contour method can make use of the knowledge derived from the apparent motion of tissue. This strengthens the principle that the movement of tissue masses should be considered within segmentation techniques, where the data facilitates it.

Furthermore, contour regularity and accuracy

was improved by using primitive shapes priors. The inherent difficulties in segmenting echocardiographic images, such as avoiding speckle noise and valve interference were also overcome by the primitive priors. Results were validated against a gold standard which was manually segmented by a clinician.

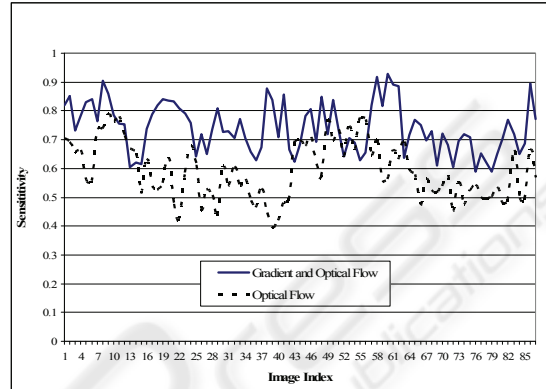


Figure 7: Sensitivity using different external energies.

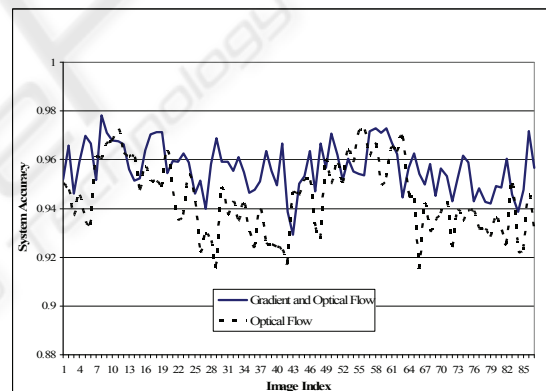


Figure 8: System Accuracy using different external energies.

ACKNOWLEDGEMENTS

This research is partially funded by the Natural Sciences and Engineering Research Council of Canada (NSERC). This support is greatly appreciated.

REFERENCES

- Amini, A., Radeva, P., Elayyadi, M. and Li, D. 1998, 'Measurement of 3D motion of myocardial material points from explicit B-surface reconstruction of tagged

- MRI data', *Medical Image Computing and Computer-Assisted Intervention*, pp. 110-118.
- Amini, A., Weymouth, T., and Jain, R. 1990, 'Using dynamic programming for solving variational problems in vision', *IEEE Pattern Analysis in Machine Intelligence*, vol. 12, no. 9, pp. 855-866.
- Barron, J., Fleet, D. and Beauchemin, D. 1994, 'Performance of optical flow techniques', *International Journal of Computer Vision*, vol. 12, no. 1, pp. 43-77.
- Canny, J. 1986, 'A computational approach to edge detection', *IEEE Pattern Analysis in Machine Intelligence*, vol. 8, no. 6, pp. 679-698.
- Choy, M. and Jin, J. 1996, 'Morphological image analysis of left ventricular endocardial borders in 2D echocardiograms', *SPIE Proceedings on Medical Imaging*, vol. 2710, pp. 852-864.
- Cohen, I. 1991, 'On active contour models and balloons', *Image Understanding*, vol. 53, no. 2, pp. 211-218.
- Cohen, L. and Cohen, I. 1993, 'Finite-element methods for active contour models and balloons for 2-d and 3-d images', *IEEE Transactions on pattern analysis and Machine Intelligence*, vol. 15, no. 11, pp. 1131-1147.
- Eusemann C., Ritman E. and Robb R. 2002, '3D visualization of endocardial peak velocities during systole and diastole', *Medical Imaging: Physiology and Function from Multidimensional Images*, vol. 4683, pp. 168-175.
- Felix-Gonzalez, N. and Valdes-Cristerna R. 2006, '3D echocardiographic segmentation using the mean-shift algorithm and an active surface model', *SPIE Medical Imaging 2006: Image Processing*, vol. 6144, pp. 1314-1319.
- Hamou, A., Osman, S. and El-Sakka, M., 2007, 'Carotid ultrasound segmentation using DP active contours', *International Conference on Image Analysis and Recognition*, vol. 4633, pp. 961-971.
- Horn, B. and Schunck, B. 1981, 'Determining optical flow', *Artificial Intelligence*, vol. 17, pp. 185-203.
- Jolly, M. 2006, 'Assisted ejection fraction in B-mode and contrast echocardiography', *Biomedical Imaging: Nano to Macro*, pp. 97-100.
- Kass, M., Witkin, A. and Terzopoulos, D. 1988, 'Snakes: Active contour models', *International Journal of Computer Vision*, vol. 1, no. 4, pp. 321-331.
- Kindermann, R and Snell, J. 1980, *Markov random fields and their applications*, American Mathematical Society, Providence, R.I.
- Mallouche, H., de Guise, J. and Goussard, Y. 1995, 'Probabilistic model of multiple dynamic curve matching for A semitransparent scene', *SPIE Vision Geometry IV*, vol. 2573, pp. 148-157.
- Mazumdar, B., Mediratta, A., Bhattacharyya, J. and Banerjee, S. 2006, 'A real time speckle noise cleaning filter for ultrasound images', *IEEE Symposium on Computer-Based Medical Systems*, pp. 341-346.
- Montagnat, J. and Delingette, H. 2000, 'Space and time shape constrained deformable surfaces for 4D medical image segmentation', *Medical Image Computing and Computer-Assisted Intervention*, vol. 1935, pp. 196-205.
- Neyman, J. and Pearson, E. 1928, 'On the use and interpretation of certain test criteria for purposes of statistical inference, part I', *Biometrika*, vol. 20a, no. 1/2, pp. 175-240.
- Papademetris, X., Sinusas, A., Dione, D. and Duncan, J. 1999, '3D cardiac deformation from ultrasound images', *Medical Image Computing and Computer-Assisted Intervention*, vol. 1679, pp. 420-429.
- Park, H. and Chung, M. 2002, 'A new external force for active contour model: virtual electric field', *Visualization, Imaging, and Image Processing*, vol. 364, pp. 90-94.
- Szeliski, R. and Tonnesen, D. 1992, 'Surface modeling with oriented particle systems', *SIGGRAPH Computer Graphics*, vol. 26, no. 2, pp. 185-194.
- Tauber, C., Batatia, H. and Ayache, A. 2008, 'Robust B-spline snakes for ultrasound image segmentation', *Springer Journal of Signal Processing Systems*.
- Williams, D. and Shah, M. 1992, 'A fast algorithm for active contours and curvature estimation', *CVGIP: Image Understanding*, vol. 55, no. 1, pp. 14-26.
- Xu, C. and Prince, J. 2000, 'Gradient vector flow deformable models', *Handbook of Medical Imaging*, pp. 159-159.
- Zhou, S., Liangbin and Chen, W. 2004, 'A new method for robust contour tracking in cardiac image sequences', *IEEE Biomedical Imaging: Nano to Macro*, vol. 1, pp. 181-184.